ChemPubSoc Europe

DOI: 10.1002/open.201800227

Open Access ChemistryOPEN Full Papers

Surface-Group-Oriented, Condensation Cyclization-Driven, Nitrogen-Doping Strategy for the Preparation of a Nitrogen-Species-Tunable, Carbon-Material-Supported Pd Catalyst

Chunshan Lu,* Xuejie Zhang, Yani Qi, Haoke Ji, Qianwen Zhu, Hao Wang, Yebin Zhou, Zhenlong Feng, and Xiaonian Li*[a]

A nitrogen-carbon framework with the thickness of several molecules was fabricated through a straightforward nitrogen-doping strategy, in which specially designed surface-oxygen-containing groups (SOGs) first introduced onto the porous carbon support were used to guide the generation of a surface-nitrogen-containing structure through condensation reactions between SOGs and the amidogen group of organic amines under hydrothermal conditions. The results indicate that different kinds of SOGs generate different types and abundances of N species. The CO-releasing groups are apt to form a high proportion of amino groups, whereas the CO_2-releasing groups, especially carboxyl and lactones, are mainly transformed into pyrrolic-type nitrogen. In the framework with dominant pyrrolic-type nitrogen, an electron-rich Pd activated site composed of Pd, pyrrolic-type N and C is built, in which electron transfer occurs from N to C and Pd atoms. This activated site contributes to the formation of electron-rich activated hydrogen and desorption of p-chloroaniline, which work together to achieve the superior selectivity about 99.90% of p-chloroaniline and the excellent reusable performance. This strategy not only provides low-cost, nitrogen-doped carbon materials, but also develops a new method for the fabrication of different kinds of nitrogen species structures.

1. Introduction

Carbon-based materials, including mesoporous/microporous carbon, carbon nanotubes (CNTs), fullerene (C_{60}), carbon nanofibers, carbon aerogel, graphene, etc., are one class of the most appealing materials used in many modern-day scientific applications.[1] Depending on the essential chemical properties of carbon element, the hybridization states of carbon atom (sp, sp^2 or sp^3) and moreover the kind and number of heteronuclear atoms bonded with carbon, these carbon-based materials exhibit versatile properties in terms of morphology, nanocarchitecture, electronic properties, chemical stablity and so on.[2] For example, two-dimensional (2D) sp^2 bonded carbon sheet arranged in a hexagonal honeycomb lattice provides graphene unique electronic, thermal and mechanical properties.[3] Heptazine or triazine heterocyclic structure linked via sp^2-bonded N atoms ($N(C)_3$ units) or –NH– groups gives carbon nitride compounds like typical C_3N_4 the special electronic, chemical and optical functionalities.[4] Consequently, the strategy by which attractive and effective properties can be obtained through modification or reconstruction of the carbon-based materials motivates researchers with great interest to explore novel bonding structure of carbon-carbon or other elements-carbon in relation to their functionality.

As the neighboring atom of carbon on the periodic table, N atom can introduce structure defects into the carbon nanostructure owing to tiny different atomic size and bond length, as well as alter the charge distribution of carbon atoms due to the difference of evident electronegativity between the N and C atom. As a result, the incorporation of nitrogen into carbon nanostructure would efficiently enhance the field emission, electronic and photochemical properties and so on. In recent years, heteroatom-doped (N, P, S, etc.) carbon materials have been attracting an increasing amount of attention in various fields such as energy conversion/storage devices,[5] photovoltaic technology,[6] adsorption/separation,[7] catalysis,[8] etc. In particular, nitrogen-doped carbon materials as the promising functional material have been recognized as metal-free catalyst for ORR,[8b,9] catalyst support for selective hydrogenation reactions,[10] and production of fuels and value-added chemicals from renewable biomass feedstock,[11] photocatalyst for hydrogen production reaction.[12] Currently, some techniques have been suggested to prepare nitrogen-doped carbon materials, such as in-situ doping method by using N-containing and C-containing organic compounds as the precursors via hydrothermal, polymerization or carbonization process.[13] This method is simpler and much more favorable to the fabrication of

[a] Prof. C. Lu, X. Zhang, Y. Qi, H. Ji, Q. Zhu, H. Wang, Y. Zhou, Z. Feng, Prof. X. Li
State Key Laboratory Breeding Base of Green Chemistry Synthesis Technology
Zhejiang University of Technology
Hangzhou 310014, China
E-mail: lcszjcn@zjut.edu.cn
xnli@zjut.edu.cn

Supporting information for this article is available on the WWW under https://doi.org/10.1002/open.201800227

uniform dispersion of nitrogen in the carbon skeleton, while the reproducibility and more vital yield of materials still is a large defiance till now.[14] Compared with this in-situ doping method, another alternative approach known as post synthesis doping is proposed to carbonize the prepared carbon materials at high temperature under nitride gas atmospheres. Although the mature and stability carbon materials can be selected as nitrogen-doping supports, thermal nitride treatment is regarded as environment unfriendly due to the released noxious gases. Therefore, it is still highly desired to develop the moderate and efficient method for nitrogen doping and accurate control of nitrogen-doped species.

Herein, we present a novel nitrogen doping strategy in which some specially designed surface oxygen containing groups (SOGs) are first introduced onto the surface of the porous carbon support via the oxidation treatments with different chemical reagents, followed by the formation of surface nitrogen-doped species through condensation reaction between these SOGs and amidogen group of organic amines under hydrothermal conditions. The molecular structures of nitrogen-containing groups strongly depend on those of the corresponding SOGs. The CN_x framework with the thickness of several molecules and tunable nitrogen species is fabricated, relying on the type and amount of surface oxygen-containing groups. Different kinds of nitrogen species exhibit different electronic properties and can be applied for various material fields. Palladium supported on the CN_x film with the main type of pyrrolic-type N presents obvious electron-rich properties as electrons transfer from N atoms to Pd toms and adjacent C atoms, which exhibits superior selectivity of 99.90% to the p-chloroaniline (p-CAN) for the chemoselective hydrogenation of p-chloronitrobenzene (p-CNB). This strategy not only provide low-cost nitrogen-doped carbon materials, but also develop a new method for the fabrication of different kinds of nitrogen species structure.

2. Results and Discussion

To selectively introduce various SOGs, activated carbon (AC (pristine)) was functionalized by exposing to liquid-phase oxidation reagents, including nitric acid, oxalic acid and hydrogen peroxide, as well as thermal treatments under nitrogen atmosphere for a purposive decrease or elimination of some kind of SOGs. The feature of various SOGs can be evaluated by He-TPD, in which all of the SOGs are thermally decomposed releasing CO_2 and/or CO at different temperatures.[15] For the qualitative and quantitative analysis of SOGs, the deconvolution method of CO_2 and CO TPD spectra proposed in the literature was employed.[15b,16] A multiple Gaussian function was used for the fitting of each spectrum. The types of SOGs were assessed by their specific decomposing temperature and the released CO_2 and/or CO. The amount of SOGs was calculated by the area of the corresponding deconvoluted peak on the basis of the external standard calibration using calcium oxalate ($CaC_2O_4{\cdot}H_2O$) as a standard sample (Figure S1). With the increase of decomposing temperature, the CO_2 curve was deconvoluted into three component peaks corresponding to carboxyl, carboxylic anhydride and lactone groups.[17] Similarly, the CO profile was deconvoluted into four component peaks corresponding to carboxylic anhydride, phenol, ether and carbonyl/quinone groups, respectively.[17b,18]

Figure 1A and 1a show CO_2 and CO TPD evolution profiles of the pretreated activated carbon (AC (pretreated)s). The type

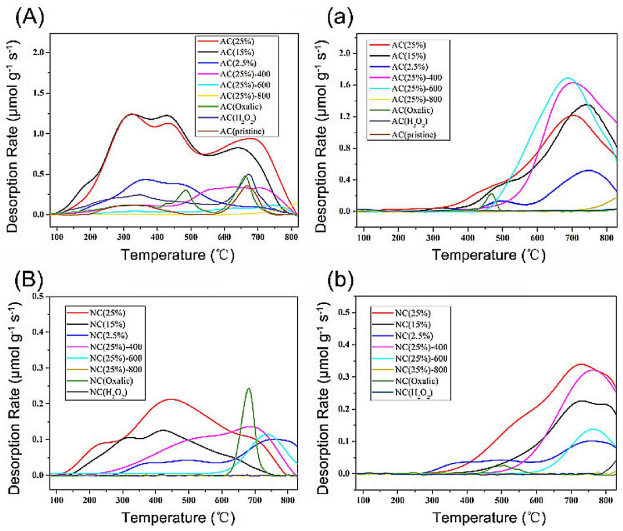

Figure 1. TPD evolution profiles of AC (pretreated)s and NC (pretreated)s: CO_2 curves (A, B); CO curves (a, b).

and amount of SOGs on each sample are summarized in Table 1 and the corresponding decomposing temperatures are listed in Table S1, obtained by the deconvolution of CO_2 and CO TPD profiles in Figure 1A and 1a. It can be seen that the AC (pristine) contains only few carboxyl and carboxylic anhydride groups. After the treatment with different concentration of nitric acid solution, all types of SOGs dramatically and nearly proportionally change as seen in the TPD curves of AC (25%), AC (15%) and AC (2.5%) the as-prepared samples were named as AC(x), where x represents the concentration of nitric acid aqueous solution. Especially for the AC (25%), the total amount of SOGs increases from 0.54 μmol/g to 11.06 μmol/g (Table 1). These results prove that various SOGs, including CO_2- and CO-releasing groups, have been introduced onto the surface of activated carbon by the liquid-phase oxidation treatment. Thermal treatment for the AC (25%) at 400 °C, 600 °C and 800 °C, respectively, selectively removes certain SOGs (Figure 1A and 1a). As can be observed in Table 1, the total amount of SOGs gradually declines as the thermal treatment temperature increases until SOGs completely eliminate at 800 °C. In fact, the decrease of SOGs at 400 °C and 600 °C mainly results from the contribution of carboxyl, carboxylic anhydride and lactone groups, and in particular, thermal treatment at 600 °C removes most CO_2-releasing groups (Figure 1A and Table 1). The CO-releasing groups like ether and phenol show not only no decrease, but also a slight increase, which is evidenced by an increase of CO amount (Figure 1a and Table 1). A possible

Table 1. Species and amounts of SOGs before (A) and after (N) hydrothermal nitridation treatment.

Sample	Carboxyl (I) [μmol/g]		Carboxylic anhydride (II) [μmol/g]		Lactone (III) [μmol/g]		Ether (IV) [μmol/g]		Phenol (V) [μmol/g]		Carbonyl/quinone (IV) [μmol/g]		Total [μmol/g]	
	A	N	A	N	A	N	A	N	A	N	A	N	A	N
AC(pristine)	0.24	\	\	\	0.30	\	\	\	\	\	\	\	0.54	\
AC(25 %)	2.17	0.21	1.89	0.19	2.09	0.59	1.58	0.38	2.81	0.58	0.52	0.20	11.06	2.15
AC(15 %)	2.21	0.18	1.92	0.05	1.55	0.51	1.44	0.16	2.22	0.40	0.37	0.16	9.71	1.46
AC(2.5 %)	0.45	\	0.70	0.20	0.06	0.06	0.55	0.04	0.66	0.18	0.20	0.07	2.62	0.55
AC(25 %)-400	0.40	\	0.76	0.53	1.13	0.20	2.03	0.11	2.72	0.59	0.71	0.30	7.75	1.73
AC(25 %)-600	0.12	\	0.17	\	0.37	0.16	1.99	0.03	2.91	0.62	0.32	0.03	5.88	0.84
AC(25 %)-800	\	\	\	\	\	\	\	\	\	\	\	\	\	\
AC(Oxalic)	0.24	\	0.26	0.02	0.49	0.11	\	\	\	\	\	\	0.99	0.13
AC(H_2O_2)	0.60	\	\	\	0.93	\	\	\	\	\	\	\	1.53	\

justification could be related to the fact that CO_2 decomposed from the SOGs with low decomposing temperature adsorbs again in the pores of activated carbon and subsequently is transformed into the SOGs with high decomposing temperature.[15b] Therefore, thermal treatment selectively removes certain CO_2-releasing groups, leaving CO-releasing groups on the surface of carbon support. In addition, the hydrogen peroxide and oxalic acid were also used as liquid treatment regents because of weak oxidation property for the former and two characteristic carboxyl groups for the latter, respectively.[19] The results exhibit that the carboxyl and lactone groups are selectively introduced onto the activated carbon which was dispersed in hydrogen peroxide aqueous solution sample (AC (H_2O_2)) with the total content of SOGs of 1.53 μmol/g, and carboxyl, lactone and carboxylic anhydride groups appear on the treated activated carbon with oxalic acid aqueous solution (AC(Oxalic)).

And then, the condensation reaction between SOGs and amidogen group of organic amines was operated by hydrothermal treatment under the condition of 200 °C for 12 h. Figure 1B and 1b show CO_2 and CO TPD evolution profiles of N-doped carbon (NC (pretreated)s). The SOGs type and amount of each sample are also concluded in Table 1. Obviously, the amount of all types of SOGs remarkably decreases, especially the CO_2-releasing groups. NC(H_2O_2) and NC(Oxalic) have nearly undetectable levels of CO_2 and CO TPD signals. However, there are still some SOGs with higher decomposing temperature like ether, phenol, carbonyl/quinone and lactone groups, on those samples treated with nitric acid and thermal treatment at 400 °C and 600 °C.

The decrease of SOGs means that the condensation reaction may have occurred and nitrogen-containing groups or structures have been formed. In order to verify this nitridation process, four samples including AC (25 %), AC (25 %)-600, AC (25 %)-800 and AC(H_2O_2) are selected out as corresponding representatives of CO_2- and CO-releasing groups, CO-releasing groups, no SOGs and CO_2-releasing groups on the basis of the type and amount of SOGs, respectively.

FT-IR and Raman were employed to investigate the changes of surface groups before and after the hydrothermal N-doping treatment. Figure 2b–e shows the Raman spectra of NC (25 %), NC (25 %)-600, NC (25 %)-800 and NC (H_2O_2). Two prominent peaks of G-band (1605 cm^{-1}) originated from crystalline graph-

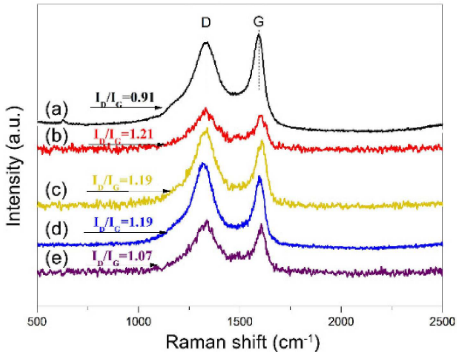

Figure 2. Raman spectra of a) AC (pristine), b) NC (25 %), c) NC (25 %)-600, d) NC (25 %)-800 and e) NC (H_2O_2).

itic/sp^2 carbon atoms and D-band (1336 cm^{-1}) induced by sp^3 hybridization,[20] can be observed in Raman spectra (Figure 2). The relative intensity ratio of D and G bands (I_D/I_G) can be used to assess the degree of disorder in carbon-based materials. The amorphous degree of all N-doped samples is higher than that of FT-IR is also a good technique for the analysis of the surface groups or chemical structure of catalyst materials. As shown in Figure 3, the absorption band at 1570, 1450 and 1106 cm^{-1} detected on AC(pristine) could be assigned to sp^2 C=C stretching vibration,[21] C–H bending vibration and C–C stretching vibration respectively,[22] which coexist in the carbon skeleton. The 3600–3200 cm^{-1} band can be linked to O–H stretching vibration probably attributed to physiosorbed water.[23] After the oxidation or thermal treatment, some changes on the adsorption bands of 1715, 1390 and 1210 cm^{-1} appear in FTIR spectra. The 1715 cm^{-1} band denoted the C=O vibration stretching of carboxyl, carboxylic anhydride, lactone and ether groups is found especially in AC(25 %).[20c,24] The 1390 cm^{-1} band represents the C–O-C stretching vibration of ether or lactone groups, which appears in AC(25 %), AC(25 %)-600 and AC(H_2O_2).[25] The intensity of 1210 cm^{-1} increases obviously in AC(25 %), AC(25 %)-600 and AC(H_2O_2), which can be the C-OH stretching vibration of carboxyl and phenol groups.[20c,24a,26] However, AC(25 %)-800 shows nearly the same absorption bands as those of AC(pristine), indicating no SOGs on the surface of AC(25 %)-800 coincided with the results of TPD. Furthermore, the condensation reaction of SOGs and EDA almost completely eliminates the bands at 1715 and 1390 cm^{-1}

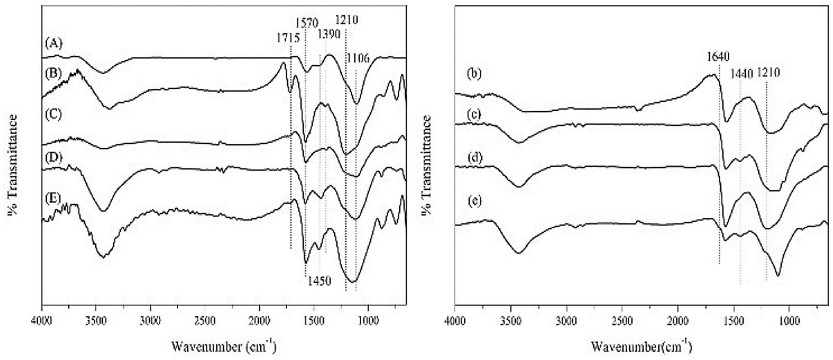

Figure 3. FTIR spectra of AC (pretreated)s and NC (pretreated)s: A) AC (pris-tine); B) AC (25 %) and b) NC (25 %); C) AC (25 %)-600 and c) NC (25 %)-600; D) AC (25 %)-800 and d) NC (25 %)-800; E) AC (H_2O_2) and e) NC(H_2O_2)

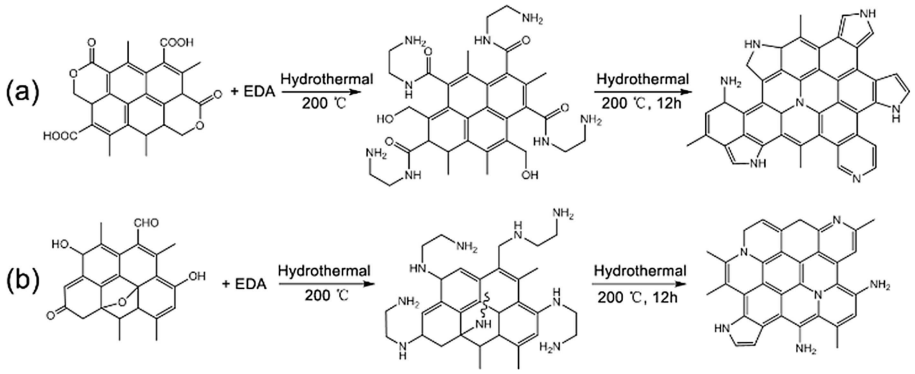

Figure 4. Potential condensation reactions on activated carbon between: a) EDA and CO_2-releasing groups (carboxyl, lactone groups); b) EDA and CO-releasing groups (carbonyl, phenol and ether groups).

(Figure 3B, C, E and Figure 3b, c, e). Accordingly, the C=O stretching vibration of 1640 cm^{-1} and the C–N vibration of 1440 cm^{-1} appear in N-doped samples, especially in NC(H_2O_2) (Fig. 3e), which can be attributed to -CONH structure judged by the combination with the 3436 cm^{-1} band[27] Although it is very difficult to determine the composite band between 1400 and 1106 cm^{-1}, the subtle difference can be seen the intensities by comparing the curves before and after condensation reaction. The intensity of 1210 cm^{-1} represented for SOGs becomes weak in NC (25 %) and NC(H_2O_2), while remains relatively strong in NC (25 %)-600 and NC (25 %)-800 (Figure 3b-e). Tran Van Khai[28] and Tingting Zhu[27] reported that the absorption band at about 1201–1246 cm^{-1} could be assigned to the C–N stretching mode in the benzenoid rings. The mentioned changes in the intensity indicate that SOGs decrease and some new nitrogen-containing groups possibly are formed.

According to the mechanism and theory in organic chemistry, condensation reaction can be occurred between SOGs and primary amine.[20c,28–29] Combined the results of TPD, Raman and FTIR, the possible surface reactions can be presented as follows (Figure 4). –OH/–OR from carboxyl, phenol, lactone and carbonyl groups, or C–O–C from ether groups, by accepting H from $–NH_2$ and formation of releasing H_2O, contributes to the formation of amide or secondary amine groups and incorporation to the carbon skeleton.[29a,30] Relying on the molecule structure of adjacent SOGs, different nitrogen-containing surface structure will be fabricated and integrated into the surface of carbon support. Moreover, in surface reaction terms, this nitrogen-containing structure should be a layer with the thickness of several molecules. The parameters of pore structure for these samples are summarized in Table S2. No obvious changes are observed in spite of the oxidation, thermal or hydrothermal treatment. Only a slight increase in surface area and total volume appears in NC (25 %)-600 and NC (H_2O_2). The similar results can also be seen in the pore distribution as shown in Figure S2b. But in general, all samples maintain nearly identical parameters of pore structure. These results should also indicate the formation of a thin CN_x film on the surface of carbon support.

Subsequently, palladium was supported on the NC (pretreated) through the impregnation method. As shown in XRD spectra (Figure 5a), there are no observable diffraction patterns of Pd species, implying that the Pd species are highly dispersed. Figure 5b shows the TEM images of these catalysts. It can be seen that Pd nanoparticles are uniformly distributed on the surface of Pd catalysts, and the average Pd particle sizes of Pd/NC (25 %), Pd/NC (25 %)-800, Pd/NC (25 %)-600 and Pd/NC(H_2O_2) are 4.15, 3.45, 2.55 and 1.75 nm, respectively (Table 2).

Figure 6 gives the XPS results of C1s and N1s spectra of Pd/AC (pristine) and Pd/NC (pretreated)s. For Pd/AC(pristine), C1s

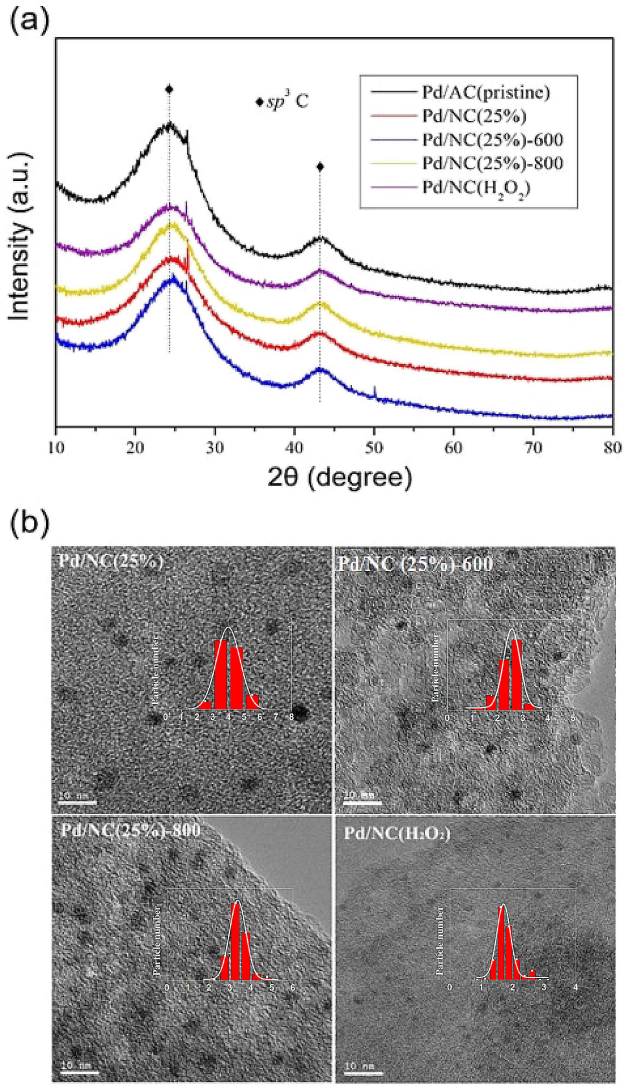

Figure 5. a) XRD patterns of Pd/AC(pristine) and Pd/NC(pretreated)s; b) TEM images of Pd/NC(pretreated)s.

Table 2. Hydrogenation of p-CNB over Pd/NC(pretreated)s [a]

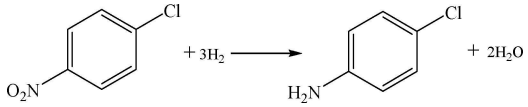

Catalyst	Pd size [nm]	Temp. [°C]	Time [min]	Conversion [%]	Selectivity [%] p-CAN	AN
Pd/NC(25%)	4.15	85	113	100.0	96.86	3.14
Pd/NC(25%)-600	2.55	85	108	100.0	94.60	5.40
Pd/NC(25%)-800	3.45	85	98	100.0	93.90	6.10
Pd/NC(H_2O_2)	1.75	85	117	100.0	99.90	0.10
Pd(2.1)/C [b]	2.1	80	92	100.0	72.73	27.27
Pd(28.4)/C [b]	28.4	80	155	100.0	99.92	0.08

[a] Reaction conditions: 0.1 g catalyst; 15.0 g p-CNB; stirring rate = 1200 rpm; 50 mL stainless steel autoclave. [b] The data is from literature,[41] reaction condition: 1.0 g catalyst, 200 g p-CNB; pH_2 = 1.0 Mpa; stirring rate = 1200 rpm; 500 mL stainless steel autoclave.

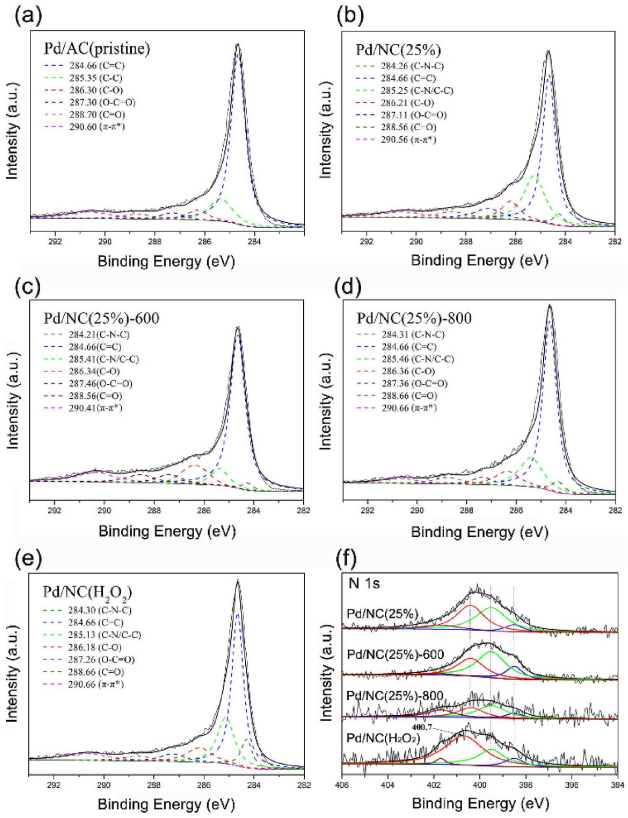

Figure 6. C1 s spectra of (a) Pd/AC(pristine), (b) Pd/NC(25%), (c) Pd/NC(25%)−600, (d) Pd/NC(25%)-800 and (e) Pd/NC(H2O2), (f) N1s spectra of Pd/NC (pretreated)s.

spectrum (Figure 6a) can be deconvoluted into six peaks at 284.66 eV, 285.35 eV, 286.30 eV, 287.30 eV, 288.70 eV and 290.6 eV corresponding to C=C(sp^2), C–C(sp^3), C–O, O-C=O, C=O, and the π–π*, respectively.[31] For all of Pd/NC(pretreated)s, additional peak appears at 284.24 ~ 284.30 eV. The most intense C1s peak located at 284.66 eV can be assigned to the sp^2-hybridized graphitic carbon (C=C) originated from the activated carbon skeleton. And the peaks centered at ~288.70 eV, ~287.30 eV and ~286.30 eV assigned to the C=O, O–C=O and C–O groups respectively, appear in all samples.[31a] The intensity of these peaks indicates the existence of trace amounts of oxygen species. Whereas SOGs of NC (pretreated)s significantly decrease after the hydrothermal N-doping process as shown in CO and CO_2 desorption curves (Figure 1B and 1b). Especially in NC(25%)-800, there is not any signals of SOGs. Hence, the signals of oxygen species in C1s spectra may be ascribed to the adsorbed CO_2/O_2/H_2O from air or the oxygen species in carbon skeleton which could keep stable even at high temperature.[15e,19] The highest BE peak (290.4 ~ 290.7 eV) of C1s is attributes to the π–π* shake-up feature, which is also one characteristic peak of carbon support. Compared with Pd/AC (pristine), there are two distinct features in C1s spectra of Pd/NC(pretreated)s. One is that the additional peak at 284.24 ~ 284.30 eV associated with C–N-C appears on all Pd/NC(pretreated)s, undoubtedly indicating the nitrogen incorporation into the carbon structure.[32] And the other is that the peak at

~285.35 eV presents inconsistent shifts among Pd/NC(pretreated)s, compared with Pd/AC(pristine). The peak at 285.2~285.4 eV in C1s spectra (Figure 6a–e) can be assigned to sp^3-hybridized carbon (C–C),[31a] on the other hand, it can also be defined as C–N group due to the disordering of graphite-like structure after embedding N atoms into carbon skeleton.[33] In fact, it is a bit difficult to specifically characterize the peak of C–C or C–N, however some positive changes can be still observed. It is worth nothing that the BE positively shifts to 285.41 eV and 285.46 eV in Pd/NC (25%)-600 and Pd/NC (25%)-800 (Figure 6c and 6d), whereas negatively shifts to 285.25 eV and 285.13 eV in Pd/NC (25%) and Pd/NC(H_2O_2) (Figure 6b and 6e). For the former, similar findings were reported by Yu,[34] Pašti[35] and our previous work,[36] in which heteroatoms may lead to a net positive charge on the carbon atoms adjacent to the heteroatoms due to spinning density and/or atomic charge density redistribution in neighboring carbon atoms. For the latter, the negative shifts may be attributed to the electron donating capability of the different N species adjacent to C atoms. More details about this point will be discussed later in this work. Thus, it seems that the characteristic peak at 285.2~285.4 eV in C1s spectra should be attributed to the C–N bond of N-doped samples (Figure 6b-e).

For further investigating the correlation of CN_x layer and carbon skeleton, the N1s XPS analysis was employed as shown in Figure 6f. The N1s spectra of all Pd/NC (pretreated)s show broad peaks between 402~398 eV resulting from an overlap of different peaks. Deconvolution of the N1s curves gives four peaks at ~398.5 eV, ~399.5 eV, ~400.4 eVand ~401.7 eV corresponding to the pyridinic-type N species, amino groups (-NH_2), pyrrolic-type N species and quaternary N species (N^+), respectively.[37] They are coded as N_{PD}, N_A, N_{PR} and N_Q in turn. As expected, it can be seen that N species on Pd/NC(pretreated)s are closely related to the different SOGs of the corresponding AC(pretreated)s. The AC (25%) with a variety of SOGs, as reflected in the stronger CO and CO_2 desorption curves in Figure 1A and 1a, displays high percentage of N_A (49.4%, Table S3) and N_{PR} (35.2%, Table S3) after the hydrothermal treatment with EDA. And, more N_A (56.9%, Table S3) are generated on the Pd/NC (25%)-600 because the CO-releasing groups (carbonyl/quinone, ether and phenol groups) were purposely introduced onto AC (25%)-600. Surprisingly, there are still trace amounts of N species (total mass content: ~0.52 wt%, Table S3) on the Pd/NC (25%)-800 with significantly higher proportion of N_Q species (21.4%, Table S3) than those of other samples. This result may be due to the incorporation of N atoms into carbon skeleton during the calcinations in N_2 atmosphere at extremely high temperature (>800 °C).[38] Carboxyl and lactone groups selectively introduced via the wet oxidation of hydrogen peroxide promote the formation of N_{PR}. N_{PR} becomes the dominant N species (64.4%, Table S3) on Pd/NC(H_2O_2). In addition, the amounts of N species of these samples are also closely related to the amounts of SOGs of the corresponding AC (pretreated)s. The amount of N species is ordered as: Pd/NC (25%) > Pd/NC (25%)-600 > Pd/NC(H_2O_2) > Pd/NC (25%)-800 (Table S3), consistent with the order of SOGs (Figure 1 and Table 1).

According to the analysis above, we found that the BE shift of C1s in C–N bond could not correspond to the changes in N1s spectra (Figure 6f). Therefore, the XPS spectra of palladium were investigated. In the inset of Figure 7, the Pd3d peaks are

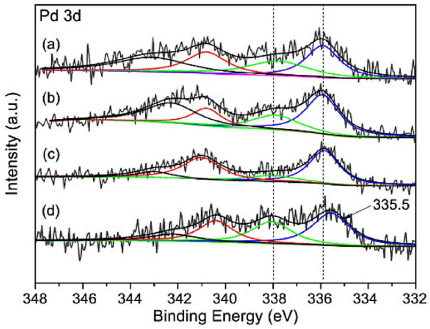

Figure 7. Pd3d spectra of a) Pd/NC (25%), b) Pd/NC (25%)-600, c) Pd/NC (25%)-800 and d) Pd/NC(H_2O_2).

deconvoluted into two pairs of doublets: $Pd3d_{3/2}$ (~340.9 eV), $Pd3d_{5/2}$ (~335.9 eV) and $Pd3d_{3/2}$ (~342.4 eV), $Pd3d_{5/2}$ (~338.0 eV), assigned to Pd^0 and Pd^{2+}, respectively.[39] It can also be seen that Pd contains with two kinds of valence states in all the samples, except for the difference in the ratio of Pd^0/Pd^{2+}. As shown in Table S4, the ratio of Pd^0/Pd^{2+} is ordered as: Pd/NC (25%)-800 ≫ Pd/NC(25%)-600 > Pd/NC(H_2O_2) ≈ Pd/NC(25%). These results are well matched with the BE shifts of C1s and N1s in Pd/NC (pretreated)s. The higher Pd^0/Pd^{2+} ratio existed in Pd/NC (25%)-800 and Pd/NC (25%)-600 may be caused by the reduction of partial Pd^{2+} to Pd^0 resulting from accepting electrons from C–N bond. It is consistent with the positive shift of C1s in C- N bond in Figure 6d and 6c. On the other hand, the BE of N1s in C–N bond shows no obvious shift as a result of the direct transformation of nitrogen species adjacent to Pd particles into quaternary N species (N^+). This oxidation reduction reaction between metal ions and surface groups on the carbon materials appears to be obvious on Pd/NC(25%)-800 in particular.[36] On the contrary, in the case of Pd/NC(25%) and Pd/NC(H_2O_2), the negative shift of C1s in C–N bond should originate from the electron donating capability of the N species (Figure 6b and 6e), especially the N_{PR}, which can be observed with higher proportion on these two samples (Table S3 and Figure 6f). But these N_{PR} may not be sufficient to reduce Pd^{2+} into Pd^0, just result in electron transfer from N to neighboring atoms.[37b] As a consequence, more electrons transfer from N atom to Pd atom and C atom in Pd/NC(H_2O_2) with the dominant N_{PR}, whereas a few electrons just transfer to C atom in Pd/NC (25%) because of a relatively small number of N_{PR}.

In a word, in the hydrothermal process, the CO-releasing groups like ether, phenol and carbonyl are transformed into large quantities of N_A, a small number of N_{PR} and N_{PD} and trace amount of N_Q. The co-existence of CO_2- and CO-releasing SOGs leads to high content of N_{PR} and N_A which show a slight electron donating capability as electrons transfer from N atoms to adjacent C atoms. Furthermore, CO_2-releasing groups such as carboxyl and lactone are mainly transformed into N_{PR}, which

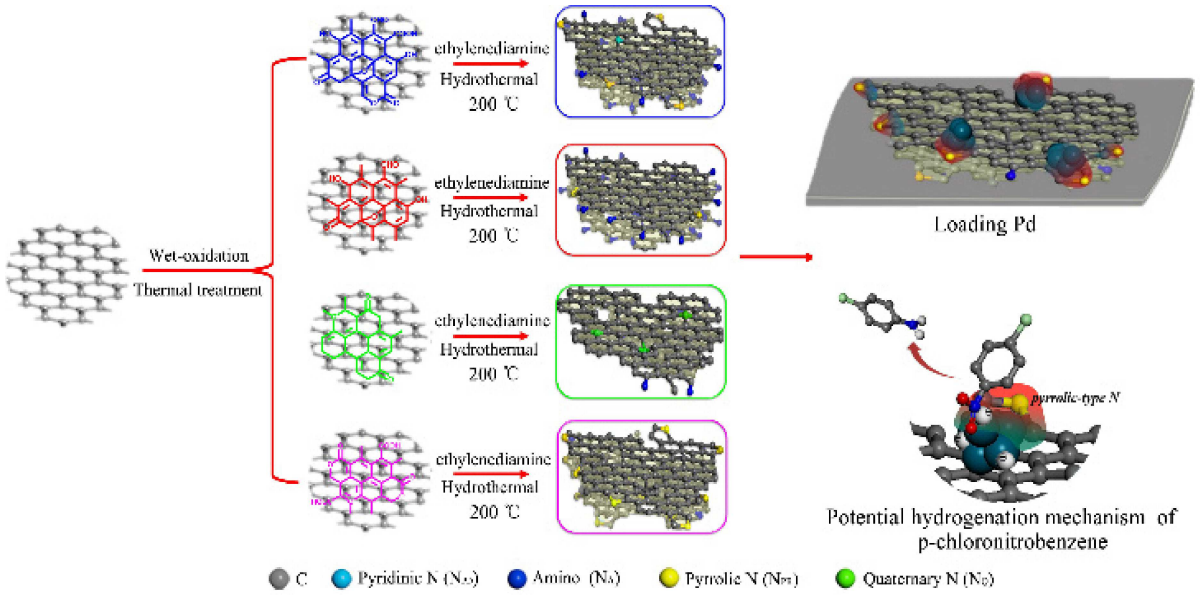

Figure 8. The surface group-oriented nitrogen doping strategy for the activated carbon supported Pd catalysts and potential selective hydrogenation mechanism of p-chloronitrobenzene.

provides more electrons to Pd atoms and adjacent C atoms. As shown in Figure 6e and Figure 6d, the BE of C–N and Pd^0 negatively shift to 285.13 eV and 335.5 eV, respectively. This stronger electron donating capability can be attributed to the special pentagonal molecule structure of pyrrole ring, which has a lone electron pair for conjugating with p-conjugated ring.[37b,40] Schematic diagram of the surface group-oriented nitrogen doping strategy is illustrated in Figure 8.

Aromatic haloamines are intensively used in the synthesis of fine chemicals.[36] The selective hydrogenation of halonitro aromatic compounds to the corresponding aromatic haloamines is considered as the most environment-friendly method. However, this reaction has been suffering from undesired hydrodehalogenation side reaction up to now. The selective hydrogenation of p-CNB to p-CAN as a model reaction was carried out under solvent-free conditions to probe the catalytic performance of Pd/NC (pretreated)s. As shown in Table 2, these Pd catalysts supported on the CN_x framework with different N-doped types show different p-CAN selectivity. The selectivity to p-CAN over Pd/NC (25%)-800 is only 93.90%. Those corresponding Pd/AC(pretreated)s catalyst without doping nitrogen demonstrates lower selectivity (Table S5). In contrast, over Pd/NC(H_2O_2) with the dominant N_{PR}, the selectivity to p-CAN reaches to 99.90% with a 100% conversion. Coq[41] and our previous works[42] have pointed out the important effect of Pd particle size on the hydrogenation of halonitro aromatic compounds. The better selectivity could be achieved only when the Pd particle size increases over 20 nm. The reason can be explained that the high proportion of terraces only existed in large Pd particle have a decisive role for the reaction barrier of hydrodehalogenation. Lyu[42] reported that the selectivity of about 99.90% was gained until the Pd particle size was larger than 28.4 nm. In contrast, the N_{PR}-modified Pd particle with the size of 1.75 nm performs the same selectivity as that of unmodified Pd particle with the size of 28 nm. In addition, the Pd/NC(H_2O_2) catalyst also exhibits remarkable catalytic performance after five cycle times without obvious deactivation under conditions comparable to literature (Figure 9). The XRD, TEM and XPS (Figure S3–5) characterization of the reused catalyst have also shown the high stability of catalyst. The aforementioned results undoubtedly demonstrate that N_{PR} tunes the electronic property of Pd activated site made up of Pd nanoparticle and N_{PR} molecule ring (Figure 8). In this structure, N atom acts as an electron donating center and transfers electrons to Pd atoms and adjacent C atoms. When adsorbed on the Pd activated site, hydrogen molecule is dissociated into electron-rich active H (H^-), which will tend to attack the N^+ core of nitro group ($O\text{-}N^+$) rather than the electron-rich Cl^- atom of C–Cl bond because the hydrogenolysis side reaction of C–Cl

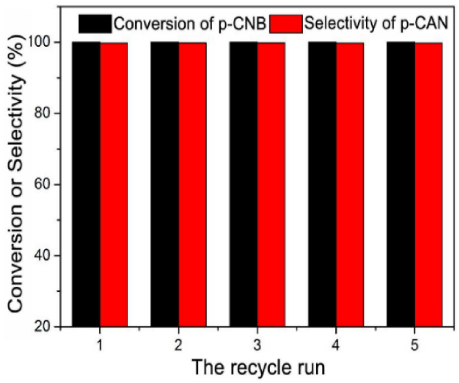

Figure 9. Reuse of Pd/NC(H_2O_2) in the hydrogenation of p-CNB. Reaction conditions: 0.1 g catalyst; 15.0 g p-CNB; stirring rate = 1200 rpm; 50 mL stainless steel autoclave.

bond is generally considered compliance with electrophilic substitution mechanism.[43] Besides, the electron-rich Pd activated site also contributes to the desorption of p-CAN molecule due to the electron donating effect of amino groups in the aromatic ring, which greatly benefit the suppression of hydrodehalogenation reaction.[44]

3. Conclusions

The certain kinds of SOGs are selectively grafted onto the activated carbon and play a crucial role of structure matrix for fabricating diverse surface N species via the condensation reaction with EDA during the hydrothermal treatment. Different kinds of SOGs generate different abundances of N species. Carboxyl, lactone and carboxylic anhydride groups react with -NH_2 group of EDA to form the amide structures (–CONH), followed by the fabrication of a N_{PR}-dominant CN_x film with the thickness of several molecules on the surface of activated carbon. In this framework, N atom transfers electrons to Pd atoms and adjacent C atoms, leading to the formation of electron-rich Pd activated site. This activated site conduces to the formation of electron-rich active H^- and the desorption of p-CAN molecule, which work together to inhibit the hydrodehalogenation side reaction. Pd/NC(H_2O_2) with dominant N_{PR} exhibits a more stable and superior selectivity of 99.90% and no obvious deactivation after five cycle times for the hydrogenation of p-CNB to p-CAN.

Experimental Section

Materials

All the chemicals and reagents were of analytical grade and were used without further purification.

Commercial activated carbon was purchased from France Arkema CECA (3sw, particle size: 250–300 mesh, N_2-BET: 980 $m^2 g^{-1}$, ash content: <3%). Nitric acid (HNO_3, 65.0~68.0 wt%, Sinopharm Chemical Reagent Co., Ltd.), Hydrogen peroxide (H_2O_2, 30 wt%, Shanghai Lingfeng Chemical Reagent Co., Ltd.), Oxalic acid dehydrate ($C_2H_2O_4{\cdot}2H_2O$, $\geq$99.9 wt%, Shanghai Lingfeng Chemical Reagent Co., Ltd.), Ammonia solution (NH_4OH, 25.0~28.0 wt%, Hangzhou Longshan Fine Chemical Co., Ltd.), 1-Chloro-4-nitrobenzene ($C_6H_4ClNO_2$, 98 wt%, Aladdin Chemistry Co., Ltd.),Palladium chloride ($PdCl_2$, Pd content $\geq$59.5 wt%, Deqing Degong Chemical Engineering Co., Ltd.), Deionized water (resistivity $>18\ \Omega\,cm^{-1}$).

SOGs Construction

Various oxygen-containing groups were introduced onto the surface of activated carbon (AC (pristine)) via pretreatment with nitric acid, oxalic acid, hydrogen peroxide and thermal treatment, respectively.

Nitric Acid Treatment

1.0 g of activated carbon was dispersed in 25.0 mL of nitric acid aqueous solution (25.0 wt%, 15.0 wt% and 2.5 wt%) in a 50 mL round bottom flask under magnetic stirring at 90 °C for 8 h. After that, these pretreated samples were collected via filtration, washed with deionized water until pH 7.0 and finally dried under vacuum at 110 °C overnight. The as-prepared samples were named as AC(x), where x represents the concentration of nitric acid aqueous solution.

Oxalic Acid Treatment

1.0 g of activated carbon was dispersed in 40.0 mL of oxalic acid aqueous solution containing 5.0 g absolute oxalic acid in a 100 mL round bottom flask, and then stirred at 50 °C for 18 h. The resulting sample was collected by filtration, washed with deionized water until pH 7.0, and finally dried under vacuum at 110 °C overnight. The obtained sample was named as AC(Oxalic).

Hydrogen Peroxide Treatment

1.0 g of activated carbon was dispersed in 15.0 mL of hydrogen peroxide aqueous solution with the concentration of 30 wt%. The rest steps were the same as the nitric acid or oxalic acid treated carbons, and the obtained sample was designated as AC(H_2O_2).

Thermal Treatment

The as-prepared sample of AC (25%) was placed in a flowing nitrogen atmosphere at 400 °C, 600 °C for 1 h and 800 °C for 2 h, respectively. The obtained samples were denoted as AC (25%)-y. y represents the temperature of calcinations.

Surface Condensation Reaction of SOGs and Ethylenediamine

The process of the surface condensation reaction was operated as follows: 1.0 g of pretreated activated carbon mentioned above (called AC (pretreated) by a joint name) was dispersed in 35.0 mL mixture solution of 10.0 mL ethylenediamine (EDA) and 25.0 mL deionized water, and then stirred at room temperature for 6 h. Subsequently, the suspension was transferred into a 50 mL Teflon-lined autoclave and hydrothermally treated at 200 °C for 12 h. The resulting modified activated carbon was collected by filtration, rinsed with deionized water until pH 7.0, and finally dried under vacuum at 80 °C overnight. The obtained N-doped sample was collectively named as NC (pretreated), in which the part of (pretreated) is labeled the same as the name of the corresponding AC (pretreated) for each sample.

Preparation of Pd/NC (Pretreated) Catalyst

The Pd catalysts supported on the N-doped carbon were prepared by the impregnation method using Pd $(NH_3)_4Cl_2$ as a precursor at room temperature. In a typical experiment, Pd $(NH_3)_4Cl_2$ aqueous solution (0.044 mol/L) could be obtained by mixing 0.4 g of $PdCl_2$ powder and 25.0 mL ammonia solution (25.0~28.0 wt%) under intensive stirring until complete dissolution, and then diluted with deionized water to 50.0 mL. Subsequently, 4.25 mL of Pd $(NH_3)_4Cl_2$ aqueous solution (0.044 mol/L) was added dropwise into the suspension of 1.0 g N-doped sample and 15.0 mL of deionized water, and then stirred continuously at room temperature for 6 h. Finally, the solid sample was filtered off immediately, washed with deionized water until pH 7.0 and then dried under vacuum at 110 °C for 5 h. The as-prepared catalysts were named as Pd/NC (pretreated), in which NC (pretreated) corresponds to the names of N-doped samples. The Pd loading for all catalysts was 2.0 wt%.

Characterization

The Fourier transform infrared (FT-IR) spectra were recorded by FT-IR (Nicolet iS50, Thermo Fisher, Madison, USA) in the range of 500 ~ 4000 cm^{-1}.Raman spectra were obtained on a Perkin-Elmer 400F Raman spectrometer with 785 nm red laser irradiation. The nitrogen adsorption and desorption isotherms at 77 K were measured on Autosorb-IQ system (Quantachrome, USA). The specific surface areas were calculated using the BET model and pore size distributions were derived from the desorption branches of the isotherms according to the HK and BJH method. X-ray diffraction (XRD) measurements were performed using an X'Pert PRO diffractometer (PNAlytical Co.) equipped with a Cu Kα radiation source that was operated at 60 kV and 55 mA. Diffraction patterns were collected at a scanning rate of 2 °/min and with a step of 0.02°.

Temperature-programmed desorption (He-TPD) was carried out in a home-built reactor equipped with a mass spectrometer (Omnistar QMS 200, Pfeiffer Instruments) for online gas analysis. About 200 mg of the dry sample was weighted accurately and put in a quartz tube (inner diameter: 10 mm). The sample was heated at a rate of 5 °C/min from room temperature to 110 °C and kept this temperature under helium atmosphere at a flow rate of 50 mL/min for 1 h in order to remove water and air that physically adsorbed in carbon microstructures. Subsequently, the sample was gradually heated to 860 °C at a rate of 5 °C/min at a helium flow rate of 50 mL/min, and then kept at 860 °C for 5 min. The released gases, mainly containing CO and CO_2, were identified by a quadrupole mass spectrometer (CO m/z: 28, CO_2 m/z: 44), and quantified by integration of the peak area on the basis of the calibration curves built by using calcium oxalate ($CaC_2O_4{\cdot}H_2O$) as a standard sample (Figure S1).

XPS analysis was collected using a Kratos AXIS Ultra DLD spectrometer with monochromatized aluminum X-ray source (1486.6 eV) for the analysis of core level signals of C1s, N1s and Pd3d with a multichannel detector. Spectra were recorded at normal emission under a vacuum of 6×10^{-9} Torr. The calibration of binding energy (BE) of the spectra was referenced to the C1s electron bonding energy at 284.66 eV arising from adventitious carbon. A Shirley-type background was subtracted from the signals. Recorded spectra were always fitted using Gauss-Lorentz curves, in order to determine the band energy of the different element core levels more accurately. The surface atomic composition ratio was calculated by using the Schofield sensitivity factors after the normalization of each individual peak area.

Catalytic Hydrogenation Tests

The catalytic hydrogenation reduction of p-CNB as a model reaction was carried out in a 50 mL stainless steel autoclave, which was charged with the desired amount of p-CNB and supported palladium catalyst under solvent-free conditions. Above all, the batch reactor was successively purged with pure N_2 and H_2 to evacuate the system, and then heated to 85 °C with 1.0 Mpa H_2 pressure and 1200 r/min stirring rate. After the reaction finished, the supported palladium catalyst was filtered from the mixture of the organics and water for the next recycle use, and the corresponding aromatic haloamine was separated by a standing and layering process. The products were periodically withdrawn from the reactor and identified by GC-MS (Agilent 5973 N) and analyzed by GC (Agilent 7890) equipped with an FID detector and a capillary column HP-5 (30 m × 0.20 mm × 0.25 μm). The quantitative analysis was conducted by area normalization method.

Acknowledgements

The work was funded by National Natural Science Foundation of China (Nos. 21476207, 21476208, and Zhejiang Provincial Natural Science Foundation of China (No. LY17B060008).

Conflict of Interest

The authors declare no conflict of interest.

Keywords: nitrogen doping strategy · nitrogen-doped carbon · selective hydrogenation · pyrrolic-type nitrogen

[1] a) X. Jia, Y. Cheng, Y. Lu, F. Wei, *ASC NANO* **2014**; b) Y. Xie, Q. Huang, B. Huang, *Carbon* **2010**, *48*, 2023–2029; c) A. Maetz, L. Delmotte, G. Moussa, J. Dentzer, S. Knopf, C. M. Ghimbeu, *Green Chem.* **2017**, *19*, 2266–2274; d) S. Wang, J. Zhang, P. Shang, Y. Li, Z. Chen, Q. Xu, *Chem. Commun. (Camb.)* **2014**, *50*, 12091–12094; e) A. Alabadi, X. Yang, Z. Dong, Z. Li, B. Tan, *J. Mater. Chem. A* **2014**, *2*, 11697–11705; f) Y. Li, J. Shen, J. Li, X. Sun, J. Shen, W. Han, L. Wang, *Carbon* **2017**, *116*, 21–32; g) W. Libbrecht, A. Verberckmoes, J. W. Thybaut, P. Van Der Voort, J. De Clercq, *Carbon* **2017**, *116*, 528–546; h) J. Shen, G. Liu, K. Huang, Z. Chu, W. Jin, N. Xu, *ACS Nano* **2016**, *10*, 3398–3409.

[2] a) T. J. Bandosz, T.-Z. Ren, *Carbon* **2017**, *118*, 561–577; b) A. Fernandez, J. C. Sanchez-Lopez, G. Lassaletta, *Carbon* **1998**, *36*, 761–764; c) V. Perazzolo, C. Durante, R. Pilot, A. Paduano, J. Zheng, G. A. Rizzi, A. Martucci, G. Granozzi, A. Gennaro, *Carbon* **2015**, *95*, 949–963; d) W. J. Ong, L. L. Tan, Y. H. Ng, S. T. Yong, S. P. Chai, *Chem. Rev.* **2016**, *116*, 7159–7329.

[3] a) S. K. Park, K. Choi, S.-H. Lee, I.-K. Oh, S. Park, H. S. Park, *Carbon* **2017**, *116*, 500–509; b) R. Kar, N. N. Patel, N. Chand, R. K. Shilpa, R. O. Dusane, D. S. Patil, S. Sinha, *Carbon* **2016**, *106*, 233–242.

[4] T. S. Miller, A. B. Jorge, T. M. Suter, A. Sella, F. Cora, P. F. McMillan, *Phys. Chem. Chem. Phys.* **2017**, *19*, 15613–15638.

[5] S. Cai, Z. Meng, H. Tang, Y. Wang, P. Tsiakaras, *Appl. Catal. B* **2017**, *217*, 477–484.

[6] G. H. Jun, S. H. Jin, S. H. Park, S. Jeon, S. H. Hong, *Carbon* **2012**, *50*, 40–46.

[7] a) B. Ashourirad, P. Arab, A. Verlander, H. M. El-Kaderi, *ACS Appl. Mater. Interfaces* **2016**, *8*, 8491–8501; b) J. Xiong, W. S. Zhu, H. P. Li, L. Yang, Y. H. Chao, P. W. Wu, S. H. Xun, W. Jiang, M. Zhang, H. M. Li, *J. Mater. Chem. A* **2015**, *3*, 12738–12747.

[8] a) Y. Lin, S. Wu, W. Shi, B. Zhang, J. Wang, Y. A. Kim, M. Endo, D. S. Su, *Chem. Commun.* **2015**, *51*, 13086–13089; b) D. W. Kim, O. L. Li, N. Saito, *Phys. Chem. Chem. Phys.* **2015**, *17*, 407–413; c) M. Hu, Z. Yao, X. Wang, *Ind. Eng. Chem. Res.* **2017**, *56*, 3477–3502; d) C. Tang, Q. Zhang, *Adv. Mater.* **2017**, *29*.

[9] a) Y. Li, Y. Zhao, H. H. Cheng, Y. Hu, G. Q. Shi, L. M. Dai, L. T. Qu, *J. Am. Chem. Soc.* **2012**, *134*, 15–18; b) X. M. Ge, A. Sumboja, D. Wuu, T. An, B. Li, F. W. T. Goh, T. S. A. Hor, Y. Zong, Z. L. Liu, *ACS Catal.* **2015**, *5*, 4643–4667.

[10] a) Y. L. Cao, S. J. Mao, M. M. Li, Y. Q. Chen, Y. Wang, *ACS Catal.* **2017**, *7*, 8090–8112; b) Z. L. Li, J. H. Liu, C. G. Xia, F. W. Li, *ACS Catal.* **2013**, *3*, 2440–2448; c) K. Chizari, I. Janowska, M. Houlle, I. Florea, O. Ersen, T. Romero, P. Bernhardt, M. J. Ledoux, C. Pham-Huu, *Appl Catal a-Gen* **2010**, *380*, 72–80; d) H. Z. Jiang, X. L. Yu, R. F. Nie, X. H. Lu, D. Zhou, Q. H. Xia, *Appl. Catal. A* **2016**, *520*, 73–81.

[11] a) S. C. Shit, R. Singuru, S. Pollastri, B. Joseph, B. S. Rao, N. Lingaiah, J. Mondal, *Catal. Sci. Technol.* **2018**, *8*, 2195–2210; b) K. Dhanalaxmi, R. Singuru, S. Mondal, L. Bai, B. M. Reddy, A. Bhaumik, J. Mondal, *ACS Sustainable Chem. Eng.* **2016**, *5*, 1033–1045.

[12] C. Han, Y. D. Wang, Y. P. Lei, B. Wang, N. Wu, Q. Shi, Q. Li, *Nano Res.* **2015**, *8*, 1199–1209.

[13] D. M. Wang, H. Xu, B. Z. Zheng, Y. Li, M. P. Liu, J. Du, D. Xiao, *Anal Methods-Uk* **2015**, *7*, 5311–5317.

[14] L. E. Jimenez-Ramirez, D. C. Camacho-Mojica, E. Munoz-Sandoval, F. Lopez-Urias, *Carbon* **2017**, *116*, 381–390.

[15] a) J. L. Figueiredo, M. F. R. Pereira, M. M. A. Freitas, J. J. M. Orfao, *Carbon* **1999**, *37*, 1379–1389; b) J. Xu, J. Zhao, J. Xu, T. Zhang, X. Li, X. Di, J. Ni, J. Wang, J. Cen, *Ind. Eng. Chem. Res.* **2014**, *53*, 14272–14281; c) L. M. Jiayun Li, Xiaonian Li, Chunshan Lu, Huazhang Liu, *Ind. Eng. Chem. Res.* **2005**, *44*, 5478–5482; d) A. Solhy, B. F. Machado, J. Beausoleil, Y. Kihn, F. Gonçalves, M. F. R. Pereira, J. J. M. Órfão, J. L. Figueiredo, J. L. Faria, P. Serp, *Carbon* **2008**, *46*, 1194–1207; e) K. Friedel Ortega, R. Arrigo, B. Frank, R. Schlögl, A. Trunschke, *Chem. Mater.* **2016**, *28*, 6826–6839.

[16] J. L. Figueiredo, M. F. R. Pereira, M. M. A. Freitas, J. J. M. Orfao, *Ind. Eng. Chem. Res.* **2007**, *46*, 4110–4115.

[17] a) J. H. Zhou, Z. J. Sui, J. Zhu, P. Li, C. De, Y. C. Dai, W. K. Yuan, *Carbon* **2007**, *45*, 785–796; b) S. Wu, G. Wen, B. Zhong, B. Zhang, X. Gu, N. Wang, D. Su, *Chinese J Catal* **2014**, *35*, 914–921.

[18] A. Valente, C. Palma, I. M. Fonseca, A. M. Ramos, J. Vital, *Carbon* **2003**, *41*, 2793–2803.

[19] S. Hermans, C. Diverchy, V. Dubois, M. Devillers, *Appl. Catal. A* **2014**, *474*, 263–271.

[20] a) M. J. Wu, Q. W. Tang, F. Dong, Z. Y. Bai, L. Zhang, J. L. Qiao, *J. Catal.* **2017**, *352*, 208–217; b) G. Abdul, X. Y. Zhu, B. L. Chen, *Chem. Eng. J.* **2017**, *319*, 9–20; c) Z. Pei, L. Li, L. Sun, S. Zhang, X.-q. Shan, S. Yang, B. Wen, *Carbon* **2013**, *51*, 156–163.

[21] J. Cheng, Y. Wang, C. Teng, Y. Shang, L. Ren, B. Jiang, *Chem. Eng. J.* **2014**, *242*, 285–293.

[22] L. Hussein, *RSC Adv.* **2016**, *6*, 13088–13100.

[23] A.-N. A. El-Hendawy, *Carbon* **2003**, *41*, 713–722.

[24] a) A. Khelifi, M. C. Almazán-Almazán, M. Pérez-Mendoza, M. Domingo-García, F. J. López-Domingo, L. Temdrara, F. J. López-Garzón, A. Addoun, *Fuel Process. Technol.* **2010**, *91*, 1338–1344; b) B. Zhang, P. Xu, Y. Qiu, Q. Yu, J. Ma, H. Wu, G. Luo, M. Xu, H. Yao, *Chem. Eng. J.* **2015**, *263*, 1–8.

[25] T. A. Saleh, *Appl. Surf. Sci.* **2011**, *257*, 7746–7751.

[26] a) H. Liu, Q. Gao, P. Dai, J. Zhang, C. Zhang, N. Bao, *J. Anal. Appl. Pyrolysis* **2013**, *102*, 7–15; b) N. Prabhu, A. K. Dalai, J. Adjaye, *Appl. Catal. A* **2011**, *401*, 1–11.

[27] T. Zhu, J. Zhou, Z. Li, S. Li, W. Si, S. Zhuo, *J. Mater. Chem. A* **2014**, *2*, 12545.

[28] T. Van Khai, H. G. Na, D. S. Kwak, Y. J. Kwon, H. Ham, K. B. Shim, H. W. Kim, *J. Mater. Chem.* **2012**, *22*, 17992.

[29] a) S. Duan, B. R. Yu, C. X. Gao, W. Yuan, J. Ma, F. J. Xu, *ACS Appl. Mater. Interfaces* **2016**, *8*, 29334–29342; b) J.-S. Oh, M. P. Kim, J.-H. Kim, H. Son, K.-H. Kim, S.-H. Kim, J.-B. Yoo, Y. Lee, G.-R. Yi, J.-D. Nam, *Polymer* **2017**, *133*, 110–118; c) E. Muñoz-Sandoval, A. J. Cortes-López, B. Flores-Gómez, J. L. Fajardo-Díaz, R. Sánchez-Salas, F. López-Urías, *Carbon* **2017**, *115*, 409–421; d) P. Janus, R. Janus, P. Kuśtrowski, S. Jarczewski, A. Wach, A. M. Silvestre-Albero, F. Rodríguez-Reinoso, *Catal. Today* **2014**, *235*, 201–209.

[30] a) T. Cordero-Lanzac, J. M. Rosas, F. J. García-Mateos, J. J. Ternero-Hidalgo, J. Palomo, J. Rodríguez-Mirasol, T. Cordero, *Carbon* **2018**, *126*, 65–76; b) W. Teng, Z. Wu, J. Fan, W.-x. Zhang, D. Zhao, *J. Mater. Chem. A* **2015**, *3*, 19168–19176; c) J. Shen, W. Huang, L. Wu, Y. Hu, M. Ye, *Composites Part A* **2007**, *38*, 1331–1336; d) L. Zhao, Z. Bacsik, N. Hedin, W. Wei, Y. Sun, M. Antonietti, M. M. Titirici, *ChemSusChem* **2010**, *3*, 840–845; e) P. Ghimire, C. Gunathilake, N. P. Wickramaratne, M. Jaroniec, *Carbon* **2017**, *121*, 408–417; f) K. M. Cho, K. H. Kim, K. Park, C. Kim, S. Kim, A. Al-Saggaf, I. Gereige, H. T. Jung, *ACS Catal.* **2017**, *7*, 7064–7069; g) X. W. Han, C. Q. Li, Y. Guo, X. H. Liu, Y. G. Zhang, Y. Q. Wang, *Appl. Catal. A* **2016**, *526*, 1–8.

[31] a) M. Smith, L. Scudiero, J. Espinal, J.-S. McEwen, M. Garcia-Perez, *Carbon* **2016**, *110*, 155–171; b) M. Varga, T. Izak, V. Vretenar, H. Kozak, J. Holovsky, A. Artemenko, M. Hulman, V. Skakalova, D. S. Lee, A. Kromka, *Carbon* **2017**, *111*, 54–61.

[32] X. J. Gong, W. J. Lu, M. C. Paau, Q. Hu, X. Wu, S. M. Shuang, C. Dong, M. M. F. Choi, *Anal. Chim. Acta* **2015**, *861*, 74–84.

[33] a) S. Liu, J. Tian, L. Wang, Y. Zhang, X. Qin, Y. Luo, A. M. Asiri, A. O. Al-Youbi, X. Sun, *Adv. Mater.* **2012**, *24*, 2037–2041; b) Y. Yamada, J. Kim, S. Matsuo, S. Sato, *Carbon* **2014**, *70*, 59–74; c) R. Zhao, X. Li, B. Sun, H. Ji, C. Wang, *J. Colloid Interface Sci.* **2017**, *487*, 297–309; d) Z. Luo, S. Lim, Z. Tian, J. Shang, L. Lai, B. MacDonald, C. Fu, Z. Shen, T. Yu, J. Lin, *J. Mater. Chem.* **2011**, *21*, 8038.

[34] D. S. Yang, D. Bhattacharjya, S. Inamdar, J. Park, J. S. Yu, *J. Am. Chem. Soc.* **2012**, *134*, 16127–16130.

[35] I. A. Pasti, N. M. Gavrilov, A. S. Dobrota, M. Momcilovic, M. Stojmenovic, A. Topalov, D. M. Stankovic, B. Babic, G. Ciric-Marjanovic, S. V. Mentus, *Electrocatalysis-Us* **2015**, *6*, 498–511.

[36] C. S. Lu, M. J. Wang, Z. L. Feng, Y. N. Qi, F. Feng, L. Ma, Q. F. Zhang, X. N. Li, *Catal. Sci. Technol.* **2017**, *7*, 1581–1589.

[37] a) R. Arrigo, M. E. Schuster, S. Abate, S. Wrabetz, K. Amakawa, D. Teschner, M. Freni, G. Centi, S. Perathoner, M. Havecker, R. Schlogl, *ChemSusChem* **2014**, *7*, 179–194; b) R. Arrigo, M. E. Schuster, Z. L. Xie, Y. M. Yi, G. Wowsnick, L. L. Sun, K. E. Hermann, M. Friedrich, P. Kast, M. Havecker, A. Knop-Gericke, R. Schlogl, *ACS Catal.* **2015**, *5*, 2740–2753.

[38] P. Ayala, R. Arenal, M. Rümmeli, A. Rubio, T. Pichler, *Carbon* **2010**, *48*, 575–586.

[39] L. M. Ombaka, P. G. Ndungu, V. O. Nyamori, *RSC Adv.* **2015**, *5*, 109–122.

[40] Q. Shi, R. Zhang, Y. Lv, Y. Deng, A. A. Elzatahrya, D. Zhao, *Carbon* **2015**, *84*, 335–346.

[41] B. Coq, A. Tijani, F. Figueras, *J. Mol. Catal.* **1991**, *68*, 331–345.

[42] J. Lyu, J. Wang, C. Lu, L. Ma, Q. Zhang, X. He, X. Li, *J. Phys. Chem. C* **2014**, *118*, 2594–2601.

[43] a) S. Iihama, S. Furukawa, T. Komatsu, *ACS Catal.* **2015**, *6*, 742–746; b) W. Shi, B. Zhang, Y. Lin, Q. Wang, Q. Zhang, D. S. Su, *ACS Catal.* **2016**, *6*, 7844–7854.

[44] H. Li, Y. Xu, H. X. Yang, F. Zhang, H. X. Li, *J. Mol. Catal. A* **2009**, *307*, 105–114.

Manuscript received: October 23, 2018
Revised manuscript received: November 16, 2018
Version of record online: ■■, ■■■

